OXFORD

ORIGINAL ARTICLE

Distinct Spatiotemporal Response Properties of Excitatory Versus Inhibitory Neurons in the Mouse Auditory Cortex

Ido Maor[1,2], Amos Shalev[1,2], and Adi Mizrahi[1,2]

[1]Department of Neurobiology and [2]The Edmond and Lily Safra Center for Brain Sciences, The Hebrew University of Jerusalem, Edmond J. Safra Campus, Givat Ram Jerusalem 91904, Israel

Address correspondence to Adi Mizrahi, Email: mizrahi.adi@mail.huji.ac.il

Abstract

In the auditory system, early neural stations such as brain stem are characterized by strict tonotopy, which is used to deconstruct sounds to their basic frequencies. But higher along the auditory hierarchy, as early as primary auditory cortex (A1), tonotopy starts breaking down at local circuits. Here, we studied the response properties of both excitatory and inhibitory neurons in the auditory cortex of anesthetized mice. We used in vivo two photon-targeted cell-attached recordings from identified parvalbumin-positive neurons (PVNs) and their excitatory pyramidal neighbors (PyrNs). We show that PyrNs are locally heterogeneous as characterized by diverse best frequencies, pairwise signal correlations, and response timing. In marked contrast, neighboring PVNs exhibited homogenous response properties in pairwise signal correlations and temporal responses. The distinct physiological microarchitecture of different cell types is maintained qualitatively in response to natural sounds. Excitatory heterogeneity and inhibitory homogeneity within the same circuit suggest different roles for each population in coding natural stimuli.

Key words: brain maps, natural sounds, parvalbumin neurons (PV neurons), two-photon targeted patch (TPTP)

Introduction

The functional organization of the brain has been studied since the early days of modern neuroscience (Mountcastle 1957; Hubel and Wiesel 1962). One type of physiological arrangement is topographic organization in which a feature of a stimulus (e.g. spatial location, sound frequency) is represented, or mapped, in a continuous manner across a specific brain area. The most extensively studied topographic maps are "inherited" from the periphery, where neighboring receptors share similar receptive fields that vary smoothly across the surface of the receptor organ. For example, the topographic arrangement of photoreceptors in the retina, which are sensitive to specific locations in the visual field, is inherited by downstream circuits along the visual pathway, including cortical areas. In the auditory system, early stations such as cochlea and brain stem are organized tonotopically. Tonotopic maps represent best frequencies (BFs) and originate from the arrangement of hair cells along the organ of Corti (Rubel and Fritzsch 2002).

Higher along the sensory hierarchy, the topographic maps that represent the periphery so strictly are often less stringent (Ohki et al. 2005; Sato et al. 2007). In audition, for example, tonotopy starts breaking down as early as primary auditory cortex (A1), such that neighboring neurons are often functionally heterogeneous (Goldstein et al. 1970; Goldstein and Abeles 1975; Hromadka et al. 2008; Bandyopadhyay et al. 2010; Rothschild et al. 2010). This heterogeneous microarchitecture is consistent with the argument that neurons in A1 are more than just frequency detectors like neurons in the cochlea and brain stem (Nelken

2008; Harris et al. 2011; Mizrahi et al. 2014). Instead, responses of neurons in A1 are non-linear (Young et al. 2005), context-dependent (Ulanovsky et al. 2003), and enable the representation of more complex "auditory features" like those found in natural sounds (Chechik and Nelken 2012). In regions higher than A1 (e.g. belt and para-belt areas, see Schreiner and Winer 2007), tonotopy fades away completely. This general transition from strictly topographic to non-topographic organization should reflect the different computations each brain region performs.

In a simplified view, the functional organization of a local circuit would reflect some specific computation (or a few) that it implements. Physiologically, neurons in A1 are well characterized by their responses to pure tones but their responses to natural sounds cannot be simply explained by their pure-tone responses (Laudanski et al. 2012). This apparent mismatch between pure tones and natural sounds may be evident in the population's functional architecture as well (Mizrahi et al. 2014). The evidence for noisy tonotopic maps in A1 has been met with skepticism both since its early reports in monkeys (Goldstein et al. 1970; Goldstein and Abeles 1975) and also in more recent work in mice. Particular skepticism has been raised following mapping results from two-photon imaging reporting local heterogeneity (Bandyopadhyay et al. 2010; Rothschild et al. 2010; Kanold et al. 2014) but see (Issa et al. 2014).

Here, to complement previous electrophysiology and calcium imaging studies, we set out to map neurons in L2/3 of A1 using two-photon targeted patch (TPTP; Margrie et al. 2003). This method maintains the superb spatial resolution of optical imaging and is superior to calcium imaging given its perfect spike detection at sub-millisecond resolution. Another advantage of TPTP is the ability to target the electrophysiological recording to specific neurons in the circuit that are fluorescently labeled (Miyamichi et al. 2013; Livneh et al. 2014). Thus, we used TPTP to map the response properties of excitatory neurons and one type of inhibitory neurons in A1, the parvalbumin fast spiking neurons (PVNs).

Cortical processing depends critically on inhibition, which acts via feed-forward and feedback interactions with excitatory neurons (Isaacson and Scanziani 2011). Inhibition is known to modulate cortical responses in space and time, shaping neuronal tuning and contributing to computations such as gain control (Wehr and Zador 2003; Seybold et al. 2015). Among the different types of interneurons, PVNs form the strongest synapse on principle cells (Hu et al. 2014). The role of inhibitory neurons in local processing is only starting to emerge. In the visual cortex, PVNs were shown to be less selective than excitatory neurons in their representation of spatial frequency or orientation (Kerlin et al. 2010; Hofer et al. 2011). These broader representations were consistent with their dense pattern of connections that pool inputs from neighboring neurons with diverse response properties (Packer and Yuste 2011). In the auditory cortex, tuning properties of PVNs are still debatable (Moore and Wehr 2013; Cohen and Mizrahi 2015; Li et al. 2015) and the organization of PVNs in cortical space has not been studied at all. To uncover the functional organization of excitatory and inhibitory neurons, we used TPTP and mapped the response properties of both PyrNs and PVNs within the same local networks in space and in time.

Materials and Methods

Animals and Surgical Procedure

All experimental procedures used in this study were approved by the Hebrew University Animal Care and Use Committee. PV–Cre (Hippenmeyer et al. 2005) and a Cre-dependent tdTomato reporter strain – Ai9 (Madisen et al. 2010) were obtained from The Jackson Laboratory. A total of 14 10–12 week-old PV-Cre, Ai9 double-heterozygous female mice (PV × Ai9) were used. 10 animals were used for the frequency response (FRA) experiment and 4 animals for the natural stimuli experiment. Mice were anesthetized with an intraperitoneal injection of ketamine and medetomidine (0.80 and 0.65 mg/kg, respectively) and a subcutaneous injection of Carprofen (4 mg/kg). Additionally, dextrose–saline was injected to prevent dehydration. Experiments lasted up to 8 h. The depth of anesthesia was assessed by monitoring the pinch withdrawal reflex. Ketamine/medetomidine was added to maintain the depth of anesthesia. The animal's rectal temperature was monitored continuously and maintained at 36 ± 1°C. For imaging and recording, a custom-made metal pin was glued to the skull using dental cement and connected to a custom stage to allow precise positioning of the head relative to the speaker (facing the right ear). The muscle overlying the left auditory cortex was removed, and a craniotomy (~2 × 2 mm) was performed over A1 (coordinates, 2.3 mm posterior and 4.2 mm lateral to bregma) as described previously (Stiebler et al. 1997; Cohen et al. 2011).

Imaging and Electrophysiology

Cell-attached recordings were obtained using targeted patch-clamp recording by a previously described procedure (Margrie et al. 2003; Judkewitz et al. 2009; Cohen and Mizrahi 2015). For visualization, the electrode was filled with a green fluorescent dye (Alexa Flour-488; 50 μM). Imaging of A1 was performed using an Ultima two-photon microscope from Prairie Technologies equipped with a ×16 water-immersion objective lens (0.8 numerical aperture; CF175; Nikon). Two-photon excitation of the electrode and somata was used at 930 nm (DeepSee femtosec laser; Spectraphysics). The recording depths of cell somata were restricted to subpial depths of 180–420 μm, documented by the multiphoton imaging. Spike waveform analysis was performed on all recorded cells (as in Cohen and Mizrahi 2015), verifying that tdTomato^{+} cells in L2/3 had faster/narrower spikes relative to tdTomato-negative (tdTomato^{−}) cells (Figure S1B, bottom).

Auditory Stimuli

Ultrasonic vocalizations (USVs) and wriggling calls (WCs) were recorded with a one-quarter inch microphone (Brüel & Kjær) from P4–P5 PV × Ai9 pups (N = 3). Vocalizations were sampled at 500 kHz and identified offline (Digidata 1322 A; Molecular Devices). The auditory stimuli were presented in a free-field configuration, using an electrostatic loudspeaker driver and a programmable attenuator (ED1, PA5, Tucker Davis Technologies). The loudspeaker (ES1) was placed ~10 cm from the right ear of the mouse. The FRA protocol was comprised from 18 pure tones (100 ms duration, 3 ms ON and OFF linear ramps) logarithmically spaced and presented at four sound pressure levels (72–42 dB SPL). Each stimulus/intensity combination was presented 12 times at a rate of 1.4 Hz (total of 864 stimuli presented in random order). The natural call protocol was composed of USVs and WCs, played-back at 3 sound pressure levels (SPL; 72–52 dB).

Data Analysis

Data analysis and statistics were performed using custom-written code in MATLAB (MathWorks). The raw voltage traces were high-pass filtered (using either a custom designed filter in MATLAB's FDATool or the Axoclamp's built-in filter at 100 Hz cut-off). Spikes were extracted from these filtered traces by thresholding. Spike times were then assigned to the local peaks of suprathreshold segments and rounded to the nearest millisecond. For each cell, we obtained a peri-stimulus time histogram (PSTH, binned at 1 ms) and determined the 100 ms response window. The response window was determined by a sliding window searching for the maximal response integral following stimulus onset (mean onset ± std was 8.8 ± 17 ms). Based on this response window, we extracted the cell's frequency-response area (FRA). Signal correlations (r_{sc}) were calculated as Pearson correlation between FRAs matrices. Temporal correlations were calculated as Pearson correlations between PSTHs within a time window of 100 ms preceding stimulus onset to 150 ms following stimulus offset.

"Neighboring neurons" were defined as being closer than 250 micron apart. For each cell we calculated seven parameters, as follows. (1) Best frequency (BF) is the tone frequency that elicited the strongest response averaged across all intensities. (2) The BF evoked response is the maximum increase in spike rates (evoked–spontaneous) across all frequency-intensity combinations. (3) The spontaneous firing rate of the cell was calculated based on the average of all 100 ms preceding each stimulus presentation. (4) The "pure-tone selectivity" of the cell is the % of all frequency-intensity combinations that evoked significant response (determined by a Mann–Whitney U test of firing rates in the "response window" compared with spontaneous firing rate, on a trial by trial basis). The selectivity index was corrected for multiple comparisons by subtracting the maximal expected number of false alarms ($72 \times 0.05 = 3.6$) from the total number of detected evoked stimuli. Therefore, the new value of response selectivity is ((#significant stimuli – 3.6)/ # stimuli) × 100. (5) Response latency is the first time point after stimulus onset at which the average spike count across all frequency-intensity combinations exceeded 2 SDs of the baseline spike rate. (6) Time to peak is the time point after stimulus onset at which average spike count (across all frequency-intensity combinations) reached maximum. (7) Response Fano factor is the measure for response reliability. For each stimulus we calculated response reliability as the evoked firing rate variance between trials divided by the square of the average firing rate. The response Fano factor of the cell is the average of this measure, across all stimuli.

For the natural stimuli protocol, response windows were determined as the 60 ms following syllable onset. Based on this response window, we extracted the cell's "syllable-selectivity." The selectivity of the cell is the % of all syllable-intensity combinations that evoked a significant response (determined by a Mann–Whitney U test of firing rates in the "response window" compared with spontaneous firing rate, on a trial by trial basis). Selectivity was calculated for WCs and USVs separately. These measurements were used for the selectivity analysis shown in supplemental figure 5. Temporal correlations were calculated as Pearson correlations between PSTHs of the full calls.

Unless explicitly stated, we used a Mann–Whitney U test for all comparisons and mean +/− std in the graphs and text. Significance was accepted at $P < 0.05$.

Results

Functional Organization of L2/3 PVNs and Pyramidal Neurons Using TPTP

To evaluate the functional organization of inhibitory versus excitatory neurons in primary auditory cortex we used in vivo TPTP recordings (Margrie et al. 2003). We chose TPTP because it is a method with high signal to noise ratio of spike detection as well as high spatial resolution (Fig. 1; Fig. S1). We recorded spiking activity from neurons in L2/3 of mice expressing tdTomato in parvalbumin neurons (PVNs; Fig. S1C). As we have previously shown in these mice, tdTomato-positive neurons are PVNs and tdTomato-negative neurons are predominantly pyramidal neurons (PyRNs) (Cohen and Mizrahi 2015). We carried out spike waveform analysis on all recorded cells, thus verifying that tdTomato$^+$ cells in L2/3 had faster/narrower spikes relative to tdTomato$^-$ cells (Figure S1B). Under ketamine anesthesia and two-photon guidance, we targeted sequentially both PVNs and PyRNs, while monitoring the precise distances between neurons. We recorded spiking responses to 18 pure-tone stimuli (3–40 kHz) at four attenuations (from 42 to 72 dB SPL). Only neurons that had tone-evoked response (determined by a two sample t-test) were included in our dataset (51–PyRNs; 59–PVNs; N = 10 mice). PyRNs had low spontaneous firing rates (range: 0–2.1 Hz; mean ± std: 0.4 ± 0.4 Hz) and short latencies to respond (range: 14–138 ms; mean ± std: 31 ± 18 ms). PVNs had significantly higher spontaneous firing rate (range: 0–6.8 Hz; mean ± std: 1.4 ± 1.4 Hz) and shorter latencies to respond (range: 13–32 ms; mean ± std: 20 ± 4 ms) as compared with PyRNs (Mann–Whitney U test: $P < 0.001$ for both comparisons). Given these physiological properties and following post-hoc histology (Fig. S1C), we verified that recordings were from primary auditory cortex, which is denoted here as A1 but may actually represent either A1 or AAF (Tsukano et al. 2016). Figure 1 shows all FRAs and several raster plots from a representative example experiment in which we recorded from 8 PVNs and 4 PyRNs within <250 microns of each other.

Tone-evoked response profiles varied widely within the local circuit, particularly for PyRNs. For example, the neighboring PyRNs in Figure 1 marked as #1 and #3 had best frequencies (BF) separated by 1.3 octaves (Fig. 1c,d; cell #1: BF = 21.7 kHz; cell # 3: BF = 8.7 kHz) . In search for local tonotopy we plotted the difference in BF as a function of the distance between all pairs of PyRNs. We found no significant relationship between pairwise BF and distances lower than 250 μm (Fig. 2a, PyRNs; $R^2 = 0.05$, $P = 0.052$) implying no tonotopy at the fine scale. In three out of the ten animals we recorded from two distinct penetration sites along the rostro-caudal axis of the auditory cortex. Pairs with larger inter-cell distances revealed clear and significant tonotopy (Fig. S1D,E; $R^2 = 0.15$, $P < 0.001$). Thus, and consistent with previous reports (see discussion), the auditory cortex of the mouse is tonotopic at a coarse scale, but tonotopy is not robust at finer scale (here <250 μm). In contrast to PyRNs, PVNs did show significant relationship between pairwise BF and pairwise distance between neurons ($R^2 = 0.1$, $P < 0.001$; Fig. 2a, PVNs). Thus, the tonotopy of PVNs at coarse scale was also maintained at fine scale (Fig. S1D,E; $R^2 = 0.09$ $P < 0.001$).

BF is only one descriptor of the neuron's response profile, which does not reflect the true breadth of response in amplitude and across frequencies. To analyze functional microarchitecture based on a more comprehensive representation of the physiological response, we calculated pairwise signal correlations (r_{sc}). As expected from the high local BF scatter,
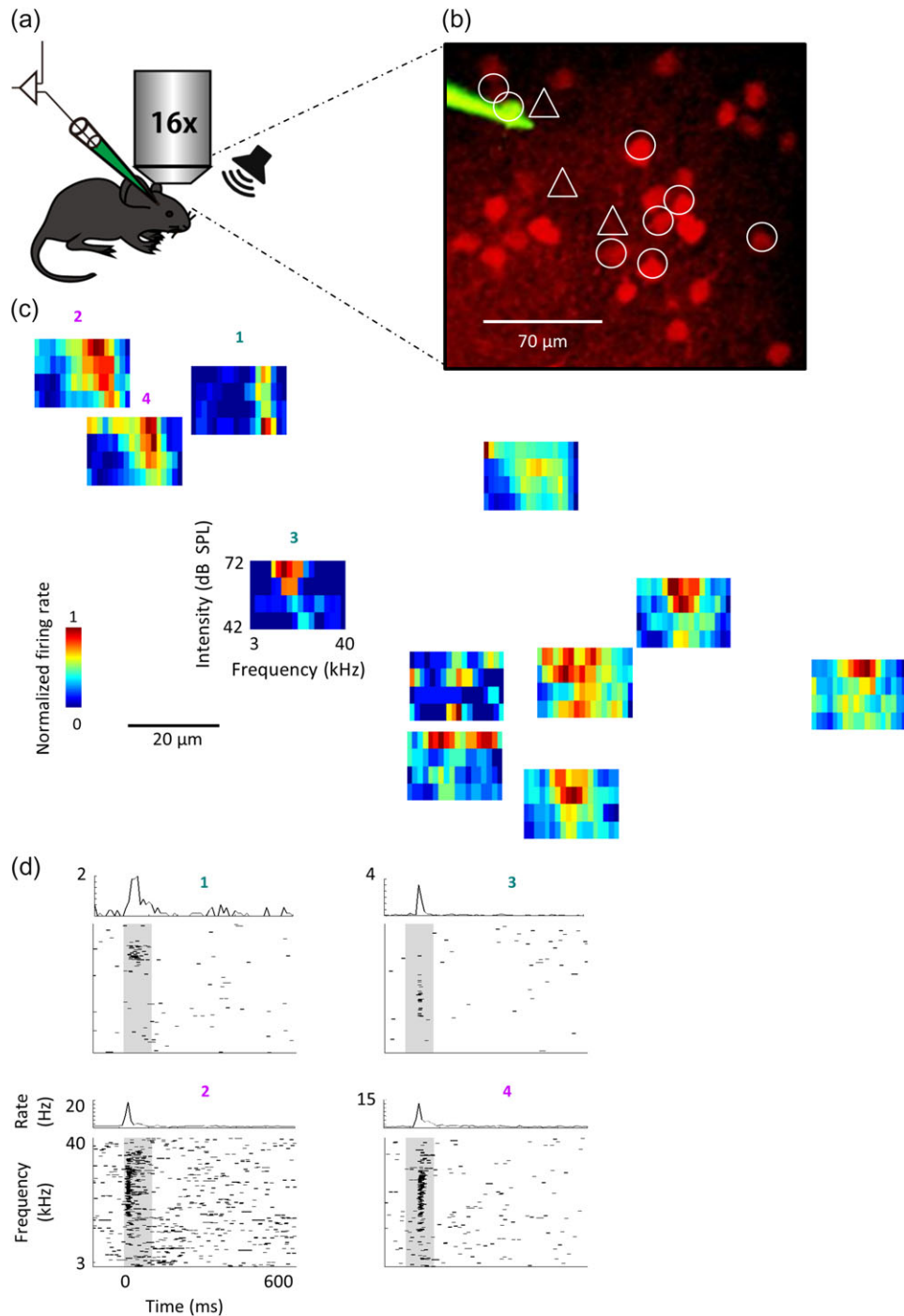
Figure 1. Mapping local circuits with two photon targeted patch (TPTP). (*a*) Schematic representation of the experimental setup for TPTP. (*b*) Representative two-photon micrograph (projection image of 120 microns) of tdTomato^{+} cells (red) and the recording electrode (Alexa Fluor-488, green). The locations of the 12 recorded neurons are marked by circles (tdTomato^{+} cells) or triangles (tdTomato– cells). (*c*) FRAs of all recorded neurons. Each FRA is drawn at the location of the neuron from which it was derived. (*d*) Raster plots and peri-stimulus time histograms (PSTH) in response to pure tones of two representative PyrNs (top, cells #1,3) and two representative PVNs (bottom, cells #2,4) from the circuit shown in *c*. Gray bars indicate the time of stimulus presentation (100 ms).

neighboring PyrNs also had highly heterogeneous FRAs (Fig. 2*b*). Overall, PyrNs were found to have a low but still positively skewed distribution of response profiles (mean $r_{sc} = 0.12 \pm 0.24$). Strikingly, PVNs exhibited much more homogeneous FRAs, 3–4 times higher than their PyrN neighbors (mean $r_{sc} = 0.4 \pm 0.19$; $P < 10^{-14}$; Fig. 2*b*). To exclude the

possibility that the high r_{sc} of PVNs stem from their intrinsic properties, we tested whether r_{sc} across groups depended on evoked firing rate, response selectivity and reliability. Although these parameters were all significantly different between cell types, they could not explain the distinct r_{sc} distributions (Fig. S2). Thus, the high r_{sc} values of PVNs reflected true similarity in
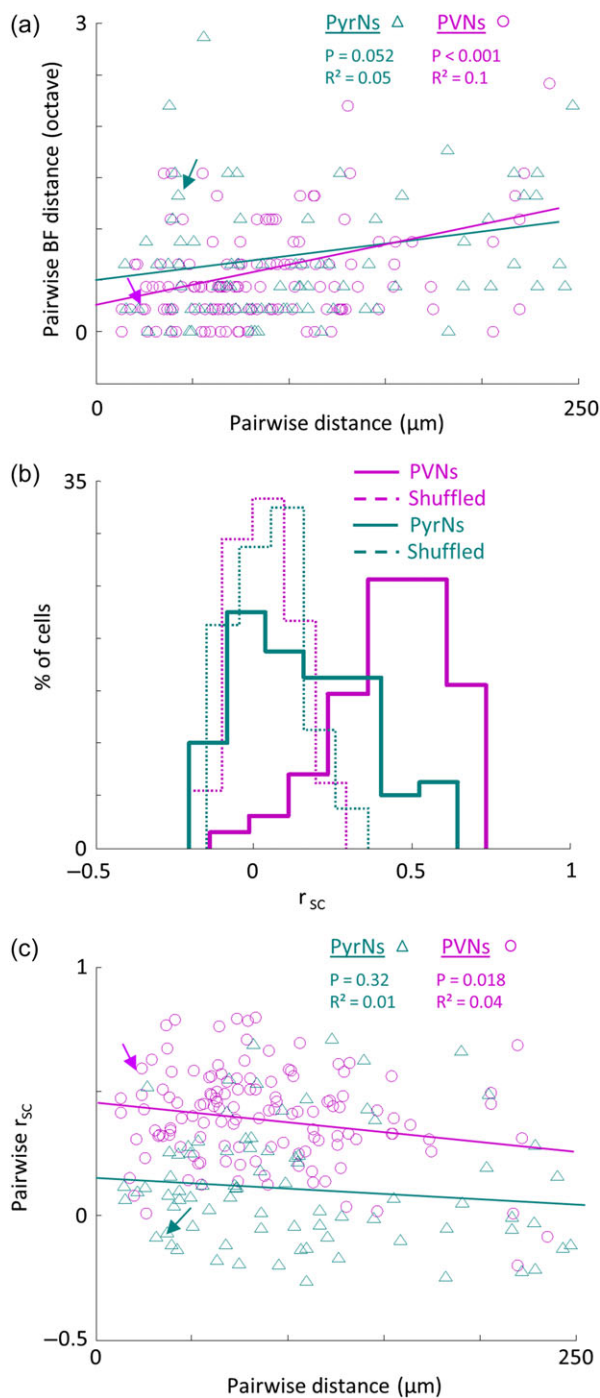
Figure 2. Distinct functional organization of PVNs and PyrNs. (*a*) Pairwise difference in BF as a function of spatial distance between pairs of PyrNs (green triangles; $n = 80$ pairs) and PVNs (magenta circles; $n = 129$ pairs). Lines indicate the best linear fit. Arrows mark the two pairs shown in Figure 1*d*. (*b*) Distribution histograms of pairwise signal correlations (r_{sc}) values between all pairs in the dataset of PyrNs (green solid line; 0.12 ± 0.24) and PVNs (magenta solid line; 0.4 ± 0.19). PyrNs and PVNs distributions are significantly different (Mann–Whitney *U*-test: $P < 0.001$). Distributions for shuffled FRAs are centered around zero and are not different between groups (dashed lines). (*c*) Pairwise r_{sc} as a function of the spatial distance between the pair. Same pairs as in *a*. PVNs but not PyrNs show a significant decrease with distance (PVNs: $R^2 = 0.04$, $P = 0.018$; PyrNs: $R^2 = 0.01$, $P = 0.32$).

receptive fields, rather than simply being an artifact of their denser FRAs or intrinsic firing properties.

To test whether PyrNs and PVNs were topographically organized, we plotted pairwise r_{sc} versus pairwise distance. Consistent with the heterogeneity of FRAs and the lack of strict local tonotopy, PyrNs showed no clear relationship between r_{sc} and distance (Fig. 2*c*; linear fit – $R^2 = 0.01$, $P = 0.32$, see also Fig. S3). On the other hand, r_{sc} values of PVNs were significantly correlated with distance (Fig. 2*c*; linear fit – $R^2 = 0.04$, $P = 0.018$, see also Fig. S3). Taken together, the picture that emerges from these data is of distinct physiological microarchitectures of the two subpopulations.

Response Properties of Neighboring Neurons in the Temporal Domain

The precision of spike timing has large implications to the neural code in general and to the auditory system in particular (Gutig and Sompolinsky 2006; David and Shamma 2013; McDermott et al. 2013; Gao and Wehr 2015). Since our mapping method is based on electrophysiology, we could test how response timing relates to the spatial position and how each subpopulation orchestrates its sensory responses over time. To do so, we first divided the spiking responses of each neuron into 20 ms time bins, thus splitting the full FRA into multiple temporal-FRA matrices for each neuron (Fig. 3*a*). Figure 3*b* shows the average pairwise r_{sc} between temporal FRAs within all time bins before and after auditory stimulation. Following the first 20 ms after stimulus onset PyrNs had positive yet low and insignificant similarity, which receded completely by 60 ms after stimulus onset (Fig. 3*b*, green bars). PVNs similarity peaked fast and remained correlated from stimulus onset and up to 60 ms after stimulus offset (Fig. 3*b*, magenta bars).

Second, we calculated the correlation between peri-stimulus time histograms (PSTHs). PSTHs of neighboring PyrNs were low (Fig. 3*c*, PyrNs) and showed no change with distance between the cells (Fig. 3*d*; $R^2 = 0.004$, $P = 0.56$). Notably, PyrNs with similar FRAs tended to be more correlated in time as well (Fig. 3*e*; $R^2 = 0.12$, $P = 0.001$). PSTH correlations between neighboring PVNs were significantly higher than those of PyrNs (Fig. 3*c*), were also not correlated with distance (Fig. 3*d*; $R^2 = 0.01$, $P = 0.16$), but were correlated with FRA similarity values (Fig. 3*e*; $R^2 = 0.08$, $P < 0.001$). Consistent with previous studies, PVNs had shorter latencies (20 ± 4 ms), and peaked faster (24 ± 6.6 ms) as compared with PyrNs (31 ± 18 ms; 36.8 ± 23.8 ms; $P < 0.001$ for both comparisons; Moore and Wehr 2013; Li et al. 2014; Cohen and Mizrahi 2015). As expected from their higher temporal correlations, latency and time to peak of the PVNs had significantly lower variability as compared with PyrNs (Fig. S4). Thus, PVNs within a local circuit behave as a homogeneous cohort not only in their responses to sound frequency and amplitude, but also over time.

Spatial Organization and Natural Stimuli

Pure tones are oversimplified stimuli lacking the complexity of real world soundscapes. We therefore investigated whether the distinct architecture of PVNs and PyrNs is a feature that will be qualitatively maintained in response to natural sounds as well. We chose pup vocalizations as the test for natural stimuli because these are sounds mice encounter in real life, even in laboratory conditions (Neunuebel et al. 2015). We used two different vocalizations that span a wide
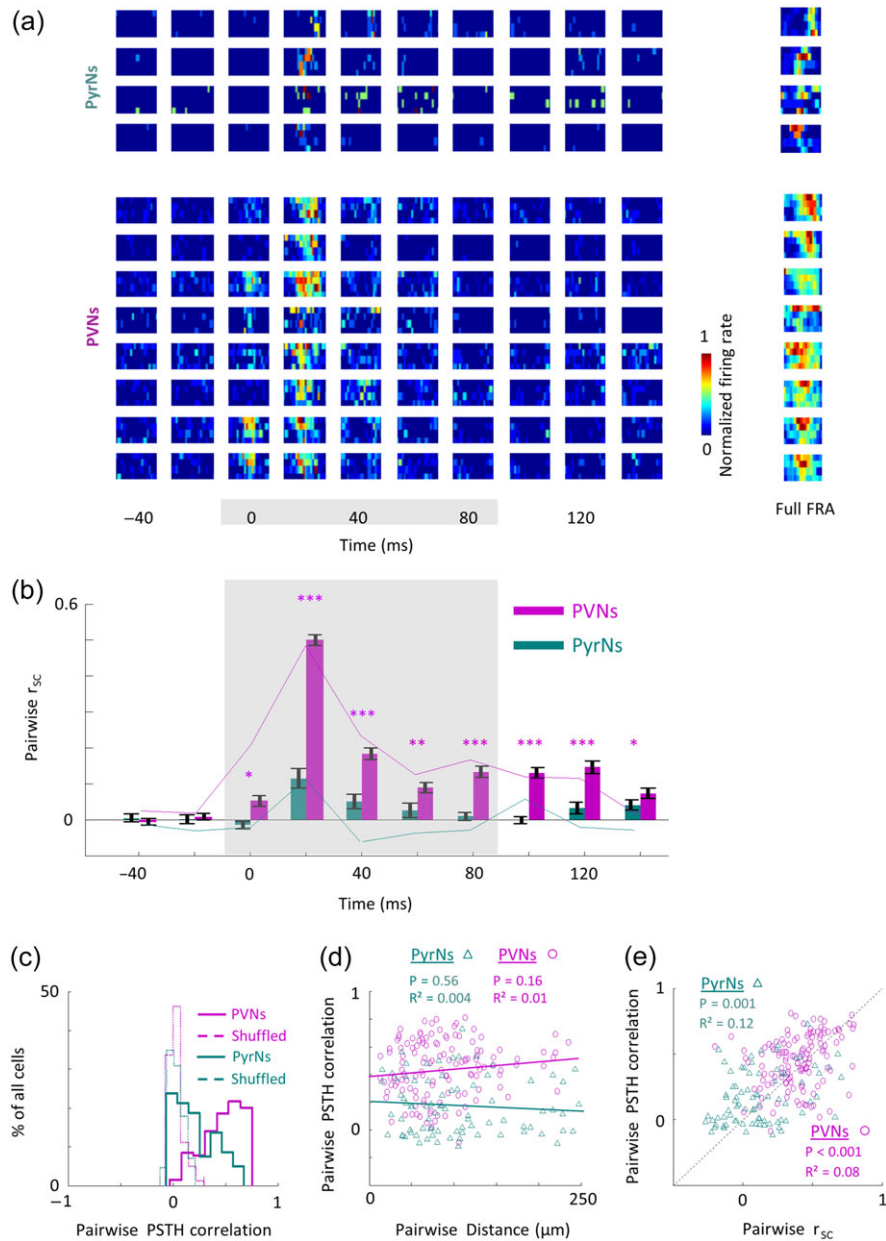
Figure 3. Distinct temporal profiles of local PVNs and PyrNs. (*a*) Temporal FRAs of all PyrNs (top panel, cells 1–4) and PVNs (bottom panel, cells 5–12) in one representative circuit from which these 12 neurons were recorded (same circuit shown in Fig. 1). Temporal segments of the FRAs are shown in sequential 20 milliseconds bins (columns) and are normalized to the maximal response across time, independently for each cell. The full FRA for each cell (calculated from 100 ms window) is shown on the right column. (*b*) r_{sc} values between temporal FRAs of all neighboring PyrNs (green bars, $n = 80$ pairs) and PVNs (magenta bars, $n = 129$ pairs). Bars show means $\pm$ SEM. Gray area indicates the time of the stimulus. The significance of correlations between PVNs or PyrNs and their shuffled FRAs is shown next to the bars (Mann–Whitney *U*-test; * $P < 0.05$, ** $P < 0.01$, *** $P < 0.001$). Colored lines corresponding to r_{sc} values of the local circuit shown in *a*. (*c*) Distribution histograms of the pairwise PSTH similarity among PyrNs (green solid line; 0.17 ± 0.2) and among PVNs (magenta solid line; 0.44 ± 0.2). PSTH correlations are significantly different between the groups (Mann–Whitney test: $P < 0.001$). Distributions for shuffled PSTHs are around zero and similar between groups (dashed lines). (*d*) Pairwise PSTH similarity values as a function of inter-neuronal distance of all pairs in the dataset. Lines indicate the best linear fit. None of the subpopulations show significant decrease with distance. (*e*) Scatter plot showing a significant correlation between pairwise r_{sc} and PSTHs for pairs of PyrNs (green triangles) and pair of PVNs (magenta circles); linear fits - PyrNs: $R^2 = 0.12$, $P = 0.001$; PVNs: $R^2 = 0.08$, $P < 0.001$.

frequency range – ultrasonic vocalizations (USV: > 20 kHz; Sewell 1970) and wriggling calls (WC: 3–20 kHz) (Geissler and Ehret 2002) at three different intensities (52–72 dB SPL). Figure 4 shows one such experiment where we sequentially patched from 11 PVNs and 10 PyrNs in the same local circuit (Fig. 4*a*). Spiking responses of PVNs and PyrNs to natural sounds were strikingly different. PVNs were significantly more responsive and more promiscuous in their response to

syllables within a sentence and the sentence as a whole (Fig. 4*b*; Fig. S5A,B).

To test whether neighboring neurons responded similarly to natural calls, we calculated pairwise correlations based on the response PSTH of each cell to both calls. Response properties of neighboring PVNs were positively correlated while those of neighboring PyrNs were not, as exemplified by the correlation matrices of the 21 neurons of Figure 4 (Fig. 4*c*). Across the data
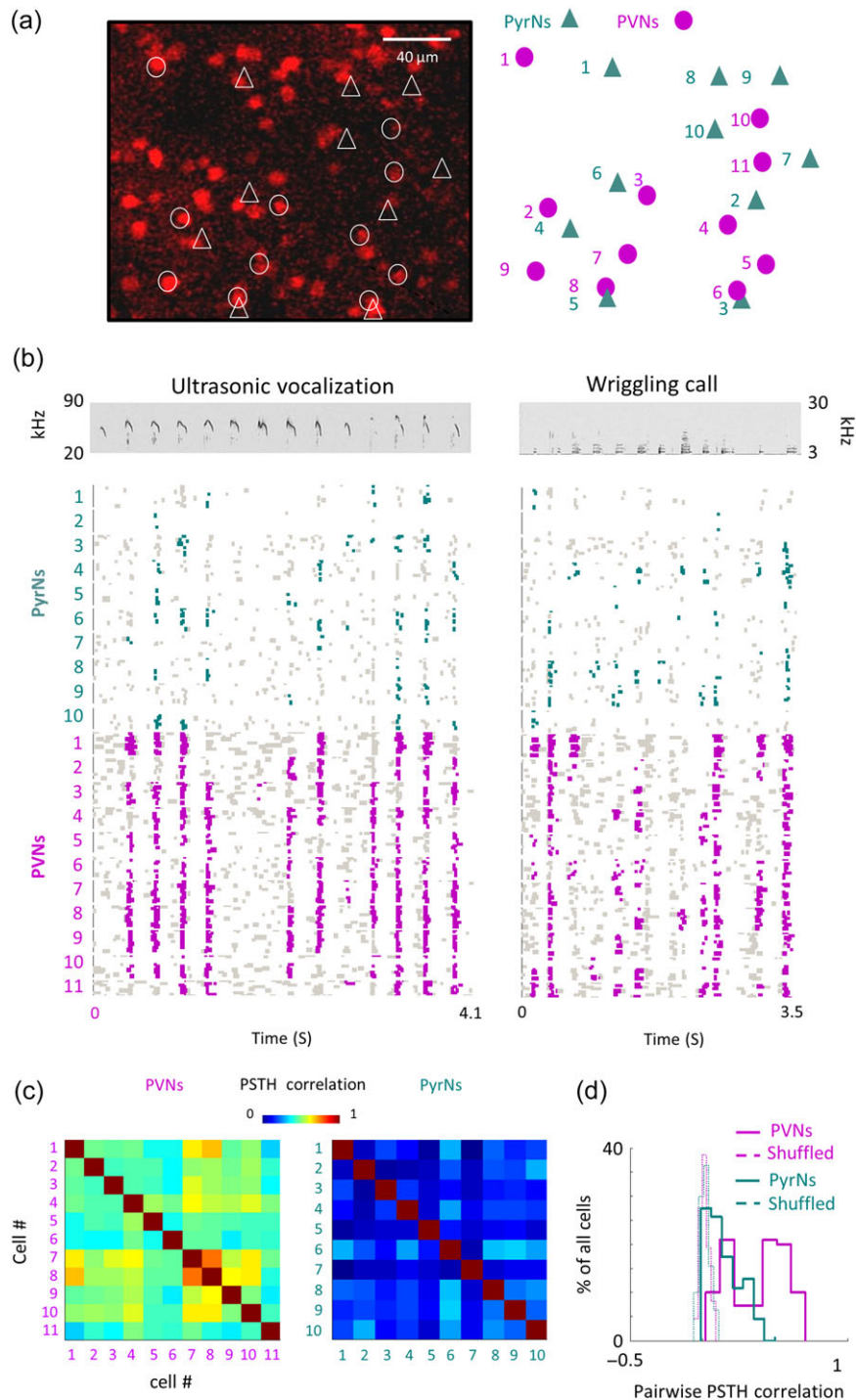
Figure 4. A representative local circuit and its responses to natural calls. (*a*) Left, two-photon micrograph (projection image of 245 microns) of tdTomato^{+} cells (red) from one representative penetration site. All recorded neurons are labeled in either circles (tdTomato^{+} cells) or triangles (tdTomato^{−} cells). Right, schematic representation of the location of neurons recorded in this site. (*b*) Top, spectrograms of the ultra-sonic vocalization (USV; left) and wriggling call (WC; right). Bottom, Raster plots of all 21 neurons (10 PyrNs and 11 PVNs) recorded from the representative circuit shown in *a* in response to the natural calls. Only responses to calls at 73 dB SPL are shown. Green and magenta dots correspond to spikes that are statistically above the baseline rate (see Methods). (*c*) Pairwise PSTH correlations among neighboring PVNs (Left) and PyrNs (Right) from the circuit shown in *a*, *b*. (*d*) Distribution histograms of PSTH correlations values between all pairs in the dataset that were recorded from the same mice. r_{sc} distributions of PyrNs (green solid line; 0.11 ± 0.12) and PVNs (magenta solid line; 0.34 ± 0.2) are significantly different (Mann–Whitney *U*-test: ***P < 0.001). Distributions for shuffled FRAs are centered around zero and are not different between groups (dashed lines).

(PyrNs: n = 109 pairs; PVNs: n = 110 pairs; N = 4 mice), PVNs were significantly more homogeneous in their responses to vocalizations as compared with their PyrN neighbors (pairwise PSTH correlations; PyrNs: 0.11 ± 0.12; PVNs: 0.34 ± 0.2; Mann–

Whitney *U* test: *P* < 0.001; Fig. 4*d*). This difference was also expressed in the tendency of neighboring neurons to respond to the same syllable in the sentence (PyrNs: 30 ± 22% cells/syllable; PVNs: 51 ± 30% cells/syllable; *P* < 0.001; Fig. 5*a*). Thus,

qualitatively, the distinct functional organization found for pure tones holds true in response to natural stimuli.

Lastly, we analyzed the relationship between different cell types sharing the same neighborhood. Inter-neuronal distance and response similarity to natural calls were not correlated in both cell types (Fig. 5b). However, PVNs and PyrNs were co-tuned to similar syllables (Fig. 5c). For a given syllable, if a PyrN in the circuit responded to it, PVNs were also responsive to that syllable. Thus, PVNs seem to "enclose" within their response properties the full breadth of neighboring PyrN responses.

Discussion

Brain mapping has gone a long way from the classical mapping of single neurons with extracellular electrodes to the more modern optical techniques (Mountcastle 1957; Hubel and Wiesel 1962; Ohki et al. 2005). Yet, all methods have their advantages and disadvantages. It is therefore important to synthesize findings across studies. Our mapping of PyrNs using TPTP shows heterogeneous architecture at local scale. This finding supports previous two-photon calcium imaging studies, which used synthetic dyes as reporters (Bandyopadhyay et al. 2010; Rothschild et al. 2010). Our data seem to contrast with another Ca^{+2} imaging work arguing that neighboring neurons' responses are highly similar (Issa et al. 2014). However, those measurements used GCamp3 as an indicator, which does not detect single spikes so critical in our dataset (Sun et al. 2013). We thus argue that the Issa et al. paper could be biased to neurons with higher spike rates missing on sparsely responsive neurons and resulting in an underestimation of the true depth of cortical heterogeneity. Indeed, pairs with high firing rates often result in higher average correlation (Fig. S2). In addition, calcium imaging does not have the temporal resolution needed to dissect out the windows of correlation we study here (100ms windows). The different temporal resolution between imaging and electrophysiology may also be a source of discrepancy.

While imaging provides superb spatial resolution to resolve single neurons (Ohki et al. 2005; Kerr and Denk 2008), it still suffers from poor reliability of spike detection. Calcium transients cannot be validated as spikes across the whole population and they are never validated for all individual experiments. In fact, variability in spike detection could be a source of bias that will skew mapping towards neurons with higher spiking activity or other patterns of spiking profiles. In auditory cortex, where responses are sparse and evoked firing rates are often low (Hromadka et al. 2008), biases due to imaging can become large. TPTP is not biased to specific cell types and has perfect spike detection. Thus, our data supports the argument that neighboring PyrNs can be heterogeneous. At the same time, we show that the PVN population is more homogeneous than PyrNs. Previous imaging mapping of A1 did not differentiate inhibitory from excitatory neurons. Assuming that PVNs were included in the imaged population we infer that some of the very high pairwise signal correlation values arising from those datasets could have their origin from PVN pairs.

PVNs in the Auditory Cortex

Sensory responses of inhibitory neurons in the auditory cortex have been studied using various techniques and in various species. The initial descriptions of PVNs in the auditory cortex were based on electrophysiological recordings in cats where they were described as having thin spikes (commonly referred to as "fast spikers"; De Ribaupierre et al. 1972). Given that PVNs are only about 10% of all neurons in the circuit (Hu et al. 2014), the absolute number of cells that could be recorded in single animals using blind methods was relatively small. Despite the small numbers, these cells were categorized as having high spontaneous and evoked firing rates (De Ribaupierre et al. 1972). Later on, the fast-spike signature in extracellular recordings was used to detect these cells with relative ease. In the cat, PVNs were shown to have short latencies, high temporal precision and broader spectral integration (Atencio and Schreiner 2008). It became increasingly clear that PVNs and PyrNs are physiologically distinct.

In the past decade, the mouse auditory system is gaining popularity as a model system. Mouse genetics offers new opportunities to target specific cell types with high specificity (Luo et al. 2008). With regard to inhibitory subtypes, mice expressing Cre recombinase in PVNs were one of the first preparations available for interneuron experimentation (Hippenmeyer et al.
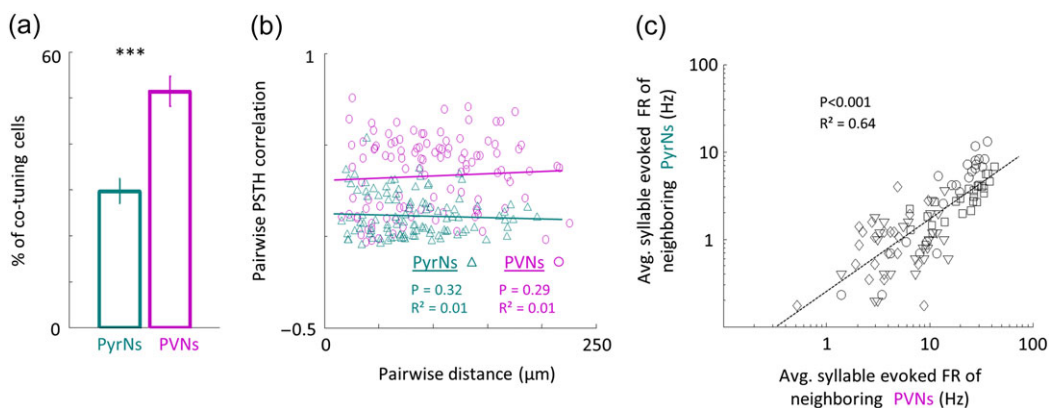
Figure 5. Distinct functional organization in responses to natural stimuli. (a) Percent of neighboring PryNs (green bar) and PVNs (magenta bar) which evoked significant responses to a specific syllable (mean±SEM. Man–Whitney U-test; *** P < 0.001). (b) Pairwise PSTH correlation values as a function of pairwise distance between PyrNs (green triangles) and PVNs (magenta circles). Lines indicate the best linear fit (PyrNs: R² = 0.01, P = 0.32; PVNs: R² = 0.01, P = 0.29). (c) Scatter plot showing linear dependency of average syllable evoked firing rate of neighboring PyrNs and its PVN neighbors (<250 microns of each other). Each marker corresponds to the average circuit response for one syllable in the sentence. The "average syllable FR" was computed for each syllable as the average firing rate across all the local cells recorded. Therefore, for each mouse there are 26 markers representing the 26 syllables. Different markers correspond to different mice. Neurons shown in Figure 4 are represented as squares. Lines indicate the best linear fit (R² = 0.64, P < 0.001).

2005). Using this mouse line, PVNs have been studied in numerous brain regions and various methods (Hu et al. 2014). In A1, channelrhodopsin-2 (ChR2) assisted targeting of PVNs initially showed that PVNs are, surprisingly, narrowly tuned (Moore and Wehr 2013). Later, however, loose patch recordings using TPTP showed that PVNs are broadly tuned compared with PyrNs (Cohen and Mizrahi 2015; Li et al. 2015). The source of these discrepancies may be due to the level of spatial resolution obtained by the two different targeting and recording methods. Our results here support the latter observations. Broadly tuned PVNs reside in local circuits and are intertwined with PyrNs that are narrowly tuned. This result holds true regardless of the average BF of the local circuit and also for natural sounds. As methods improve, the detailed inhibitory landscape of the cortex continues to be discovered.

PVNs: Different Circuits, Same Function?

We found that PVNs in the auditory cortex are locally homogeneous. This homogeneity in space and time leads us to argue that the PVNs react nonspecifically to the general activity that is being processed by the local circuitry. To a large extent, these findings were already inferred following connectivity mapping experiments in somatosensory cortex, showing dense PyrN-to-PVN synaptic connectivity (Pala and Petersen 2015) and high PVN-to-PVNs electrical coupling (Galarreta and Hestrin 2002). Moreover, imaging in the visual cortex strengthened this hypothesis. Using in vivo imaging in V1 of the mouse, Hofer and colleagues found higher pairwise correlation between neighboring PVNs as compared with neighboring PyrNs (Hofer et al. 2011). Scholl and colleagues used calcium imaging in V1 to measure the physiological similarity in the representation of binocular disparity. They compared between similarity of individual PVNs or individual excitatory neurons to their neighboring neuronal populations. PVNs had disparity selectivity bias that matched that of the local population activity (Scholl et al. 2015). These two papers suggest a similar (i.e. general) function for PVNs for different computations in the same network. Our data supports an argument that there is a similar role for PVNs in different cortical networks. In fact, this argument may extend beyond the cortex. PVNs in completely different brain regions, like the olfactory bulb and entorhinal cortex, show similar results. For example, olfactory bulb PVNs have relatively wide receptive fields and are involved in functions that sense the general activity within the local network (Kato et al. 2013; Miyamichi et al. 2013; Buetfering et al. 2014).

Given that PVNs in A1 are broadly tuned and are highly coherent, they are poised to function globally and in a powerful way. Global functions may take multiple forms. For example, normalization has been suggested as a canonical global computation (Carandini and Heeger 2013). In the auditory cortex, PVNs could mediate spectro-temporal contrast gain control (Rabinowitz et al. 2012). Another example for a global function is neuromodulation. Indeed, PVNs were shown to play a key role in relaying neuromodulatory information in associative fear learning (Letzkus et al. 2011) and in context-dependent neuromodulation (Cohen and Mizrahi 2015). Moreover, PVNs have been shown to modulate the local activity when the animals are in different cognitive states (Zhou et al. 2014; Schneider et al. 2014). Taken together, the PVN population has highly promiscuous responses to both simple and complex sounds, presumably being sensitive to the general activity in the network and, as a result, well positioned to function globally. Yet, global is a relative concept. Despite their promiscuity

and homogenous organization, PVNs can provide different types of inhibition (e.g. division or subtraction), depending on the local network properties (Seybold et al. 2015).

Cortical Space and the Temporal Code

Using TPTP we could extract the precise temporal structure of neuronal responses. Precise spike timing has large implications to the neural code in the auditory system (David and Shamma 2013; McDermott et al. 2013; Gao and Wehr 2015). In particular, the precise timing of inhibition is known to be extremely efficient in cessation (or relief) of spiking activity of excitatory neurons (Wehr and Zador 2003; Isaacson and Scanziani 2011; Letzkus et al. 2015). We show that PyrNs are temporally diverse at the fine scale. Thus, the neural code carried by local PyrNs is even sparser than suggested by spectral responsiveness alone. In complete contrast, PVNs remain correlated throughout sensory stimulation (Fig. 3). These results suggest that one possible mechanism for the efficient inhibition in A1 is the correlated activity of the inhibitory neighbors.

The spectro-temporal homogeneity of PVNs may have a large impact on the temporal sensitivity of PyrNs. For example, neurons in A1 are known to be sensitive to the recent history of the stimulus – a phenomenon known as stimulus specific adaptation (SSA; Ulanovsky et al. 2003; Hershenhoren et al. 2014). In SSA, the responses to frequently-presented stimuli decrease, while responses to rare stimuli are hardly affected. Inhibition could conceivably play a role in such processes. Indeed, PVNs have recently been shown to contribute to SSA by inhibiting, nonspecifically, the response of PyrNs to both frequent and rare stimuli (Natan et al. 2015).

Heterogeneous and Homogenous Circuits as Substrates for Plasticity

Brain maps are able to and often do change in response to experience (Dragoi et al. 2001; Rosenzweig et al. 2003; Feldman and Brecht 2005; Schreiner and Polley 2014). Even simple association of specific frequencies with reward or punishment can alter the response properties of single neurons and the gross tonotopic map in A1 (Recanzone et al. 1993; Rutkowski and Weinberger 2005). Moreover, neurons in A1 can rapidly adjust their receptive field while engaged in a behavioral task, most likely due to top-down influences (Fritz et al. 2003; Yin et al. 2014). It has already been hypothesized that heterogeneous microarchitectures can be advantageous for experience-dependent plasticity at the circuit level (Stettler and Axel 2009). In a locally heterogeneous circuit, where every neuron has immediate access to diverse sets of inputs, synaptic strengthening or weakening can have immediate impact on receptive fields without the need for dramatic rewiring. This principle could be useful when the brain learns to process natural sounds that are comprised of diverse frequency components (Theunissen and Elie 2014). In mothers, for example, responses of PyrNs to the natural calls emitted by pups are enhanced. Strikingly, this plasticity is channeled via changes in the inhibition/excitation balance of the local circuit (Marlin et al. 2015; Elyada and Mizrahi 2015). The homogeneous architecture of PVNs intertwined within heterogeneous networks of PyrNs could be one substrate for such plastic changes to occur fast and reliably.

Supplementary Material

Supplementary material can be found at: http://www.cercor.oxfordjournals.org/

Funding

Notes

References

Atencio CA, Schreiner CE. 2008. Spectrotemporal processing differences between auditory cortical fast-spiking and regular-spiking neurons. J Neurosci. 28:3897–3910.

Bandyopadhyay S, Shamma SA, Kanold PO. 2010. Dichotomy of functional organization in the mouse auditory cortex. Nat Neurosci. 13:361–368.

Buetfering C, Allen K, Monyer H. 2014. Parvalbumin interneurons provide grid cell-driven recurrent inhibition in the medial entorhinal cortex. Nat Neurosci. 17:710–718.

Carandini M, Heeger DJ. 2013. Normalization as a canonical neural computation. Nat Rev Neurosci. 14:152–152.

Chechik G, Nelken I. 2012. Auditory abstraction from spectro-temporal features to coding auditory entities. Proc Natl Acad Sci U S A. 109:18968–18973.

Cohen L, Mizrahi A. 2015. Plasticity during motherhood: changes in excitatory and inhibitory layer 2/3 neurons in auditory cortex. J Neurosci. 35:1806–1815.

Cohen L, Rothschild G, Mizrahi A. 2011. Multisensory integration of natural odors and sounds in the auditory cortex. Neuron. 72:357–369.

David SV, Shamma SA. 2013. Integration over multiple timescales in primary auditory cortex. J Neurosci. 33:19154–19166.

De Ribaupierre F, Goldstein MH Jr, Yeni-Komshian G. 1972. Intracellular study of the cat's primary auditory cortex. Brain Res. 48:185–204.

Dragoi V, Rivadulla C, Sur M. 2001. Foci of orientation plasticity in visual cortex. Nature. 411:80–86.

Elyada YM, Mizrahi A. 2015. Becoming a mother-circuit plasticity underlying maternal behavior. Curr Opin Neurobiol. 35:49–56.

Feldman DE, Brecht M. 2005. Map plasticity in somatosensory cortex. Science. 310:810–815.

Fritz J, Shamma S, Elhilali M, Klein D. 2003. Rapid task-related plasticity of spectrotemporal receptive fields in primary auditory cortex. Nat Neurosci. 6:1216–1223.

Galarreta M, Hestrin S. 2002. Electrical and chemical synapses among parvalbumin fast-spiking GABAergic interneurons in adult mouse neocortex. Proc Natl Acad Sci U S A. 99:12438–12443.

Gao X, Wehr M. 2015. A coding transformation for temporally structured sounds within auditory cortical neurons. Neuron. 86:292–303.

Geissler DB, Ehret G. 2002. Time-critical integration of formants for perception of communication calls in mice. Proc Natl Acad Sci U S A. 99:9021–9025.

Goldstein MH Jr, Abeles M. 1975. Note on tonotopic organization of primary auditory cortex in the cat. Brain Res. 100:188–191.

Goldstein MH Jr, Abeles M, Daly RL, McIntosh J. 1970. Functional architecture in cat primary auditory cortex: tonotopic organization. J Neurophysiol. 33:188–197.

Gutig R, Sompolinsky H. 2006. The tempotron: a neuron that learns spike timing-based decisions. Nat Neurosci. 9:420–428.

Harris KD, Bartho P, Chadderton P, Curto C, de la Rocha J, Hollender L, Itskov V, Luczak A, Marguet SL, Renart A, et al. 2011. How do neurons work together? Lessons from auditory cortex. Hear Res. 271:37–53.

Hershenhoren I, Taaseh N, Antunes FM, Nelken I. 2014. Intracellular correlates of stimulus-specific adaptation. J Neurosci. 34:3303–3319.

Hippenmeyer S, Vrieseling E, Sigrist M, Portmann T, Laengle C, Ladle DR, Arber S. 2005. A developmental switch in the response of DRG neurons to ETS transcription factor signaling. PLoS Biol. 3:e159.

Hofer SB, Ko H, Pichler B, Vogelstein J, Ros H, Zeng H, Lein E, Lesica NA, Mrsic-Flogel TD. 2011. Differential connectivity and response dynamics of excitatory and inhibitory neurons in visual cortex. Nat Neurosci. 14:1045–1052.

Hromadka T, Deweese MR, Zador AM. 2008. Sparse representation of sounds in the unanesthetized auditory cortex. PLoS Biol. 6:e16.

Hu H, Gan J, Jonas P. 2014. Interneurons. Fast-spiking, parvalbumin(+) GABAergic interneurons: from cellular design to microcircuit function. Science. 345:1255263.

Hubel DH, Wiesel TN. 1962. Receptive fields, binocular interaction and functional architecture in the cat's visual cortex. J Physiol. 160:106–154.

Isaacson JS, Scanziani M. 2011. How inhibition shapes cortical activity. Neuron. 72:231–243.

Issa JB, Haeffele BD, Agarwal A, Bergles DE, Young ED, Yue DT. 2014. Multiscale optical Ca2+ imaging of tonal organization in mouse auditory cortex. Neuron. 83:944–959.

Judkewitz B, Rizzi M, Kitamura K, Hausser M. 2009. Targeted single-cell electroporation of mammalian neurons in vivo. Nat Protoc. 4:862–869.

Kanold PO, Nelken I, Polley DB. 2014. Local versus global scales of organization in auditory cortex. Trends Neurosci. 37:502–510.

Kato HK, Gillet SN, Peters AJ, Isaacson JS, Komiyama T. 2013. Parvalbumin-expressing interneurons linearly control olfactory bulb output. Neuron. 80:1218–1231.

Kerlin AM, Andermann ML, Berezovskii VK, Reid RC. 2010. Broadly tuned response properties of diverse inhibitory neuron subtypes in mouse visual cortex. Neuron. 67:858–871.

Kerr JN, Denk W. 2008. Imaging in vivo: watching the brain in action. Nat Rev Neurosci. 9:195–205.

Laudanski J, Edeline JM, Huetz C. 2012. Differences between spectro-temporal receptive fields derived from artificial and natural stimuli in the auditory cortex. PLoS One. 7:e50539.

Letzkus JJ, Wolff SB, Luthi A. 2015. Disinhibition, a circuit mechanism for associative learning and memory. Neuron. 88:264–276.

Letzkus JJ, Wolff SB, Meyer EM, Tovote P, Courtin J, Herry C, Luthi A. 2011. A disinhibitory microcircuit for associative fear learning in the auditory cortex. Nature. 480:331–335.

Li LY, Ji XY, Liang F, Li YT, Xiao Z, Tao HW, Zhang LI. 2014. A feedforward inhibitory circuit mediates lateral refinement of sensory representation in upper layer 2/3 of mouse primary auditory cortex. J Neurosci. 34:13670–13683.

Li LY, Xiong XR, Ibrahim LA, Yuan W, Tao HW, Zhang LI. 2015. Differential receptive field properties of parvalbumin and

somatostatin inhibitory neurons in mouse auditory cortex. Cereb Cortex. 25:1782–1791.

Livneh Y, Adam Y, Mizrahi A. 2014. Odor processing by adult-born neurons. Neuron. 81:1097–1110.

Luo L, Callaway EM, Svoboda K. 2008. Genetic dissection of neural circuits. Neuron. 57:634–660.

Madisen L, Zwingman TA, Sunkin SM, Oh SW, Zariwala HA, Gu H, Ng LL, Palmiter RD, Hawrylycz MJ, Jones AR, et al. 2010. A robust and high-throughput Cre reporting and characterization system for the whole mouse brain. Nat Neurosci. 13:133–140.

Margrie TW, Meyer AH, Caputi A, Monyer H, Hasan MT, Schaefer AT, Denk W, Brecht M. 2003. Targeted whole-cell recordings in the mammalian brain in vivo. Neuron. 39:911–918.

Marlin BJ, Mitre M, D'Amour J A, Chao MV, Froemke RC. 2015. Oxytocin enables maternal behaviour by balancing cortical inhibition. Nature. 520:499–504.

McDermott JH, Schemitsch M, Simoncelli EP. 2013. Summary statistics in auditory perception. Nat Neurosci. 16:493–498.

Miyamichi K, Shlomai-Fuchs Y, Shu M, Weissbourd BC, Luo L, Mizrahi A. 2013. Dissecting local circuits: parvalbumin interneurons underlie broad feedback control of olfactory bulb output. Neuron. 80:1232–1245.

Mizrahi A, Shalev A, Nelken I. 2014. Single neuron and population coding of natural sounds in auditory cortex. Curr Opin Neurobiol. 24:103–110.

Moore AK, Wehr M. 2013. Parvalbumin-expressing inhibitory interneurons in auditory cortex are well-tuned for frequency. J Neurosci. 33:13713–13723.

Mountcastle VB. 1957. Modality and topographic properties of single neurons of cat's somatic sensory cortex. J Neurophysiol. 20:408–434.

Natan RG, Briguglio JJ, Mwilambwe-Tshilobo L, Jones SI, Aizenberg M, Goldberg EM, Geffen MN. 2015. Complementary control of sensory adaptation by two types of cortical interneurons. Elife. 4. doi:10.7554/eLife.09868.

Nelken I. 2008. Processing of complex sounds in the auditory system. Curr Opin Neurobiol. 18:413–417.

Neunuebel JP, Taylor AL, Arthur BJ, Egnor SE. 2015. Female mice ultrasonically interact with males during courtship displays. Elife. 4. doi:10.7554/eLife.06203

Ohki K, Chung S, Ch'ng YH, Kara P, Reid RC. 2005. Functional imaging with cellular resolution reveals precise micro-architecture in visual cortex. Nature. 433:597–603.

Packer AM, Yuste R. 2011. Dense, unspecific connectivity of neocortical parvalbumin-positive interneurons: a canonical microcircuit for inhibition? J Neurosci. 31:13260–13271.

Pala A, Petersen CC. 2015. In vivo measurement of cell-type-specific synaptic connectivity and synaptic transmission in layer 2/3 mouse barrel cortex. Neuron. 85:68–75.

Rabinowitz NC, Willmore BD, Schnupp JW, King AJ. 2012. Spectrotemporal contrast kernels for neurons in primary auditory cortex. J Neurosci. 32:11271–11284.

Recanzone GH, Schreiner CE, Merzenich MM. 1993. Plasticity in the frequency representation of primary auditory cortex following discrimination training in adult owl monkeys. J Neurosci. 13:87–103.

Rosenzweig ES, Redish AD, McNaughton BL, Barnes CA. 2003. Hippocampal map realignment and spatial learning. Nat Neurosci. 6:609–615.

Rothschild G, Nelken I, Mizrahi A. 2010. Functional organization and population dynamics in the mouse primary auditory cortex. Nat Neurosci. 13:353–360.

Rubel EW, Fritzsch B. 2002. Auditory system development: primary auditory neurons and their targets. Ann Rev Neurosci. 25:51–101.

Rutkowski RG, Weinberger NM. 2005. Encoding of learned importance of sound by magnitude of representational area in primary auditory cortex. Proc Natl Acad Sci U S A. 102: 13664–13669.

Sato TR, Gray NW, Mainen ZF, Svoboda K. 2007. The functional microarchitecture of the mouse barrel cortex. PLoS Biol. 5: e189.

Schneider DM, Nelson A, Mooney R. 2014. A synaptic and circuit basis for corollary discharge in the auditory cortex. Nature. 513:189–194.

Scholl B, Pattadkal JJ, Dilly GA, Priebe NJ, Zemelman BV. 2015. Local integration accounts for weak selectivity of mouse neocortical parvalbumin interneurons. Neuron. 87:424–436.

Schreiner CE, Polley DB. 2014. Auditory map plasticity: diversity in causes and consequences. Curr Opin Neurobiol. 24: 143–156.

Schreiner CE, Winer JA. 2007. Auditory cortex mapmaking: principles, projections, and plasticity. Neuron. 56:356–365.

Sewell GD. 1970. Ultrasonic communication in rodents. Nature. 227:410.

Seybold BA, Phillips EA, Schreiner CE, Hasenstaub AR. 2015. Inhibitory actions unified by network integration. Neuron. 87:1181–1192.

Stettler DD, Axel R. 2009. Representations of odor in the piriform cortex. Neuron. 63:854–864.

Stiebler I, Neulist R, Fichtel I, Ehret G. 1997. The auditory cortex of the house mouse: left-right differences, tonotopic organization and quantitative analysis of frequency representation. J Comp Physiol A. 181:559–571.

Sun XR, Badura A, Pacheco DA, Lynch LA, Schneider ER, Taylor MP, Hogue IB, Enquist LW, Murthy M, Wang SS. 2013. Fast GCaMPs for improved tracking of neuronal activity. Nat Commun. 4:2170.

Theunissen FE, Elie JE. 2014. Neural processing of natural sounds. Nat Rev Neurosci. 15:355–366.

Tsukano H, Horie M, Hishida R, Takahashi K, Takebayashi H, Shibuki K. 2016. Quantitative map of multiple auditory cortical regions with a stereotaxic fine-scale atlas of the mouse brain. Sci Rep. 6:22315.

Ulanovsky N, Las L, Nelken I. 2003. Processing of low-probability sounds by cortical neurons. Nat Neurosci. 6:391–398.

Wehr M, Zador AM. 2003. Balanced inhibition underlies tuning and sharpens spike timing in auditory cortex. Nature. 426: 442–446.

Yin P, Fritz JB, Shamma SA. 2014. Rapid spectrotemporal plasticity in primary auditory cortex during behavior. J Neurosci. 34:4396–4408.

Young ED, Yu JJ, Reiss LA. 2005. Non-linearities and the representation of auditory spectra. Int Rev Neurobiol. 70: 135–168.

Zhou M, Liang F, Xiong XR, Li L, Li H, Xiao Z, Tao HW, Zhang LI. 2014. Scaling down of balanced excitation and inhibition by active behavioral states in auditory cortex. Nat Neurosci. 17: 841–850.